The Journal of Korean Vacuum Science & Technology
Vol. 2, No. 2, October 1998, pp. 107~117

Epitaxy of Si and $Si_{1-x}Ge_x$(001) by ultrahigh vacuum ion-beam sputter deposition

N.-E. Lee and J. E. Greene*

School of Metallurgical and Materials Engineering
Sungkyunkwan University, 300 Chunchun-dong, Suwon, Kyunggi 440-746, Korea
**Materials Science Department, the Coordinated Science Laboratory, and the Materials Research Laboratory, University of Illinois, 1101 W. Springfield Ave., Urbana, IL 61801, USA*
(Received August 13, 1998)

Abstract – Epitaxial undoped and Sb-doped Si films have been grown on Si(001) substrates at temperatures T_s between 80 and 750°C using energetic Si in ultra-high-vacuum Kr^+-ion-beam sputter deposition(IBSD). Critical epitaxial thicknesses t_c, the average thickness of epitaxial layers, in undoped films were found to range from 8 nm at T_s=80°C to >1.2 μm at T_s=300°C while Sb incorporation probabilities σ_{Sb} varied from unity at $T_s \leq 550$°C to ≃0.1 at 750°C. These t_c and σ_{Sb} values are approximately one and one-to-three orders of magnitude, respectively, higher than reported results achieved with molecular-beam epitaxy. Plan-view and cross-sectional transmission electron microscopy, high-resolution x-ray diffraction, channeling and axial angular-yield profiles by Rutherford backscattering spectroscopy for epitaxial $Si_{1-x}Ge_x$(001) alloy films ($0.15 \leq x \leq 0.30$) demonstrated that the films are of extremely high crystalline quality. Critical layer thicknesses h_c, the film thickness where strain relaxation starts, in these alloys were found to increase rapidly with decreasing growth temperature. For $Si_{0.70}Ge_{0.30}$, h_c ranged from ≃35 nm at T_s=550°C to ≃650 nm at 350°C compared to an equilibrium value of 8 nm.

1. INTRODUCTION

Sputter deposition offers potential advantages for the growth of epitaxial layers. These include uniform deposition over large areas and the inherent ability to exploit the use of low-energy ion/surface interactions during film growth. Low-energy ion irradiation has been shown to provide enhanced adatom surface mobilities [1], lower "epitaxial temperatures"[2], increased dopant incorporation probabilities [3], and better control over dopant depth distributions (including δ-doped layers) [3, 4]. Nevertheless, there have been relatively few reports of sputter-deposited group-IV semiconductors with good electrical properties.

A serious problem associated with Si growth by molecular beam epitaxy (MBE) is the strong tendency for dopant surface segregation and very low incorporation probabilities leading to difficulty in controlling depth distributions and obtaining abrupt doping profiles [5]. Solutions to these problems have primarily involved the use of low-energy accelerated ions to trap dopants in near-surface sites, thereby increasing dopant incorporation probabilities [3-5] and low-temperature epitaxy.

The growth of epitaxial $Si_{1-x}Ge_x$ has been extensively investigated due to the possibility of bandgap engineering fully-strained alloys for the development of new electronic and optoelectronic devices compatible with conventional Si-based fabrication technology [6]. Alloy deposition temperatures for various growth techniques are typically ≥550°C. The primary problems associated with $Si_{1-x}Ge_x$ alloy growth are strain-induced surface roughening [7, 8], surface segregation of Ge [9], and limited strained-layer thicknesses due to relaxation through misfit dislocation generation [10-15].

Compressive in-plane strain associated with the growth of $Si_{1-x}Ge_x$ epitaxial films on Si is relieved through two primary pathways. For $Si_{1-x}Ge_x(001)$ alloys with lower Ge concentrations (e.g., $x \lesssim 0.3$) grown at lower temperatures ($T_s \lesssim$ 500°C depending upon x), relaxation tends to occur through plastic deformation resulting from misfit dislocation generation and the accompanying formation of threading dislocations [10, 11, 16]. In contrast, alloys with higher Ge concentrations and/or higher deposition temperatures grow via a Stranski-Krastanov (S-K) mechanism and partially relax through coherent 3D island formation in which the strain is accommodated by elastic deformation near the island edges [16], followed by the formation of misfit dislocations. Critical film thicknesses for both misfit dislocation generation, h_c [10-15] and the 2D → 3D S-K transition, $h_{S\text{-}K}$ [7], are strongly dependent upon the Ge concentration. There are experimental indications that h_c [14, 15] and $h_{S\text{-}K}$ [8] are dependent upon film growth temperature although systematic measurements of $h_c(T_s)$ and $h_{S\text{-}K}(T_s)$ are lacking. Decreasing epitaxial growth temperatures offers solutions to some of the problems listed above through kinetic inhibition of both Ge surface segregation and the nucleation of misfit dislocations.

In the present experiments, Sb incorporation probabilities σ_{Sb} during *in-situ* Sb doping and critical epitaxial thicknesses t_c in undoped and Sb doped films were measured. And the crystalline quality and critical layer thicknesses h_c of $Si_{1-x}Ge_x$ heteroepitaxial layers grown on Si(001) at low temperatures (300-550°C) were measured.

2. EXPERIMENTAL PROCEDURE

All film growth experiments were conducted in an ultra-high vacuum (UHV) three-chamber load-locked stainless-steel system shown schematically elsewhere [18]. The growth chamber is cryo-pumped with a base pressure of 1×10^{-10} Torr and contains facilities for *in-situ* RHEED and residual gas analysis while the ion-pumped analytical chamber is equipped with an Auger electron spectrometer (AES). Sputtering is carried out using modified UHV Kaufman-type double-grid multi-aperture broad ion-beam sources with provisions for *in-situ* spatial adjustment.

High-purity energetic Si, Si:Sb, and Ge beams were generated by bombarding undoped float-zone (FZ) Si targets, Czochralski (CZ) Sb-doped ($n=3.5 \times 10^{18}$ cm^{-3}, 0.021 Ω-cm) Si wafers, and undoped Ge targets, respectively, using 1-keV-Kr^+ ion beams. TRIM Monte Carlo computer simulations which can estimate the energy, flux, and angular distributions of sputtered atoms as well as backreflected Kr neutrals were used to optimize a system geometry. A system geometry was chosen so that the average energy of Si(Ge) atoms incident at the substrate surface is 18(15) eV while backreflected Kr contributes only 0.04(0.06) eV per deposited Si(Ge) with $J_{Kr}/J_{Si(Ge)} \simeq 0.003$ (0.01). Based upon molecular dynamics simulations of Si growth on Si(001)-2×1 using energetic condensing species, an interesting energy range without ion-induced damage is between 10 and 50 eV. [19]

The substrates used in these experiments were $15 \times 15 \times 0.5$ mm^3 plates cleaved from B-doped p-type Si(001) wafers with a resistivity of 1-2 Ω-cm. Substrate cleaning consisted of degreasing followed by a UV ozone treatment. The wafers were then H-passivated by dipping in dilute HF, and immediately inserted into the vacuum system. Final substrate preparation consisted of degassing at 200°C for 1 h followed by desorption at 650°C for 10 s immediately prior to initiating film growth. RHEED patterns were 2×1 with sharp Kikuchi lines. No residual C or O was detected by AES.

Chemical analyses of doped and undoped films were carried out using a Cameca IMS-5 SIMS

operated with a 10 keV O^+ for metallic impurities. A 12.5 keV Cs^+ ion beam was used to analyze for $^{217}CsKr^+$ metastable molecular ions (Kr detection limit $\simeq 5\times10^{17}$ cm^{-3}) and for Sb where, in both cases, concentrations were determined by comparison to ion-implanted standards. Temperature-dependent (50-300 K) resistivity and Hall measurements on Sb-doped samples were conducted using the van der Pauw technique with a 10 kG magnetic field. Ohmic contacts were formed by rapid thermal annealing of evaporated Sb-Ge-Au alloys. RBS 001 and 011 channeling and axial yield profiles provided additional quantitative measures of crystalline quality. High-resolution XRD measurements for determining composition of alloys films and relaxation status were performed using a four-axis diffractometer. Plan-view TEM and XTEM analyses were also carried out to determine the status of film relaxation.

3. RESULTS AND DISCUSSION

3.1 Growth of undoped and Sb-doped Si(001) layers

A. Si(001) layers grown at $T_s\geq300$°C

All undoped 1-μm-thick Si(001) films grown at $T_s = 300$°C were found, using a combination of TEM and XTEM, to be high-quality single crystals. High-resolution (110) XTEM images exhibited {111} lattice fringes which were continuous across the substrate/film interface with no indication of disorder. Plan-view (004) bright-field micrographs were featureless with no evidence of extended defects.

SIMS analyses of undoped Si layers revealed no detectible metallic impurities such as such as Fe, Cr, Ni, Mo, and W (detection limits 5×10^{15}-1×10^{16} cm^{-3}). The elimination of such contamination, inherent in previous Si IBSD growth experiments [20], was due primarily to minimizing the sputtering of chamber walls and fixtures by stray Kr^+ ions through focussing of the beam using a combination of a post-extraction unipotential electrostatic ion lens and Si apertures. The use of an external circular filament for beam neutralization eliminated W contamination which is a problem during IBSD using Kaufman-type ion-sources with immersed-wire neutralizers.

Oxygen and carbon impurity levels in undoped and Sb-doped Si films were also measured using SIMS. For films grown at $T_s\geq500$°C, the C concentration C_C was typically 2×10^{17} cm^{-3} while the O concentration C_O was below detection limits ($\simeq1\times10^{18}$ cm^{-3}). These levels are comparable to those of bulk CZ Si substrates in which C_C is 1×10^{17} cm^{-3} and C_O is 1×10^{18} cm^{-3}, respectively. As the film growth temperature was decreased to T_s=300°C, C_C and C_O increased to 5×10^{17} cm^{-3} and 5×10^{18} cm^{-3}, respectively, due to decreased associative desorption rates during deposition.

Incorporated Kr concentrations C_{Kr} were also found to be less than SIMS detection limits, 5×10^{17} cm^{-3}, at all Si film growth temperatures. Based upon TRIM results for the present geometry with J_{Kr}/J_{Si}=0.003 and $\langle E_{Kr}\rangle$ 15 eV, the Kr incorporation probability σ_{Kr} in our experiments is $<10^{-3}$ at all film growth temperatures. This is consistent with previous Ar^+ incorporation results in Si(001) at room temperature for which σ_{Ar} was reported to be 4×10^{-4} and 1.5×10^{-3} with $\langle E_{Ar}\rangle$= 20 and 100 eV, respectively [21].

In addition to the investigation of undoped Si films, the behavior of Sb dopant incorporation during *in-situ* Sb doping was investigated. Calibrated SIMS measurements were used to measure the Sb concentration C_{Sb}, and hence to determine the Sb incorporation probability σ_{Sb} in both 1-μm-thick single-layer and multilayer samples. Each layer in the multilayer samples was 200 nm thick, grown at a different Ts value (the highest temperature layers were grown first), and separated from adjacent layers by epitaxial 100-nm-thick

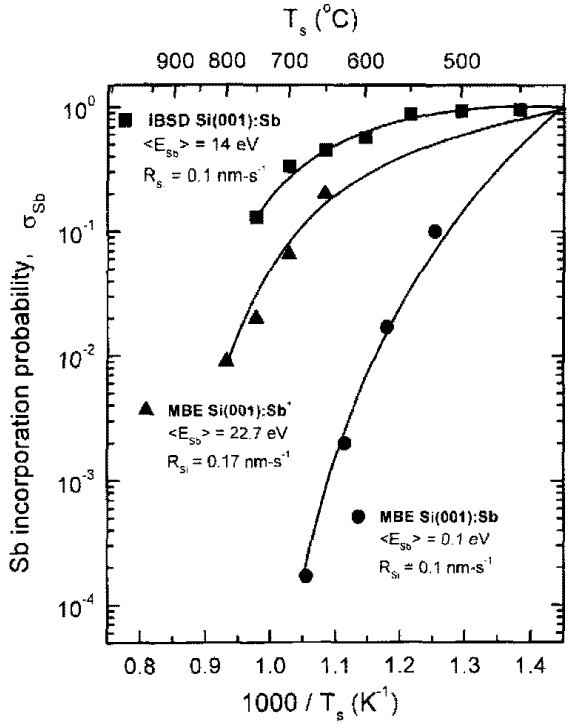

Fig. 1. Sb incorporation probability σ_{Sb} in IBSD homoepitaxial Si(001) as a function of film growth temperature T_s. Data for accelerated ion-doped (ref. 3) and coevaporatively Sb_4 doped (ref. 22) MBE Si(001) are also shown for comparison.

buffer layers grown at 300°C for which σ_{Sb} is known to be unity. σ_{Sb} vs T_s results are shown in Fig. 1 together with results for co-evaporatively doped [22] and ion doped [3] MBE Si films.

σ_{Sb} values in Fig. 1 for the IBSD films range from 0.1 at 750°C to essentially unity for T_s 550°C. This is 10 to 10^3 times larger than obtained by thermal doping during MBE where Sb surface segregation is extremely strong and Sb is lost from the segregated layer by desorption [4, 22]. In fact, $\sigma_{Sb}(T_s)$ data for IBSD are higher than for Sb ion doping with an acceleration potential V_{Sb}=50 V during MBE Si [3]. The ion flux in the MBE experiment was composed of approximately 23% Sb_1^+, 54% Sb_2^+, and 23% Sb_4^+ corresponding to an average energy per accelerated Sb of 22.7 eV. We believe that the increase in σ_{Sb} observed during IBSD is primarily due to the additional effect of Sb recoil implantation by energetic sputter-deposited Si atoms. SIMS profiles of both the multilayer and the single layer IBSD films showed no evidence of Sb surface segregation.

All Sb-doped IBSD films were found to be n-type with room temperature carrier concentrations n ranging from 6.9×10^{17} at T_s = 700°C to 2×10^{18} cm^{-3} at T_s = 300°C. Values of the Sb donor concentration N_{Sb} were obtained by a nonlinear least squares fit of measured n(T) data using the charge neutrality equation for the case in which there is a single donor level with $N_{Sb}\gg N_a$ and $N_{Sb}\gg p$,

$$n=\frac{N_{Sb}}{1+2exp\left[(-(E_f-E_{Sb}))/kT\right]}-N_a^-+p. \quad (1)$$

E_f in equation (1) is the Fermi energy which is related to n through the expression $n/N_c=F_{1/2}(E_f/kT)$ where $F_{1/2}$ is a Fermi integral [23]. N_c, the effective density of states in the conduction band, is $2(2\pi m^*kT/h^2)^{2/3}M_c$. The effective mass m^*=0.33 m_e is essentially independent of T, and M_c=6 is the number of equivalent conduction band minima.

The Sb donor concentrations N_{Sb} obtained from the n(T) Hall data analyzed using equation (1) were found to be in good agreement with chemical concentrations C_{Sb} obtained from calibrated SIMS analyses of Si films grown at $T_s\geq350$°C as shown on Fig. 2. Decreasing T_s to 300°C, however, results in $\simeq$30% of the i[illegible] Sb becoming electrically inactive due to the presence of the higher background C and O concentrations and/or residual ion-induced damage undetectable by TEM.

Room-temperature electron mobilities μ_e(300K) as a function of n are plotted in Fig. 3. Comparing the results indicates that IBSD layers grown at $T_s\geq400$°C exhibit mobilities equivalent to bulk values. At lower film growth temperatures, μ_e(300K) values decreased, yielding ratios with respect to bulk of $\simeq$0.78 and $\simeq$0.70 at T_s=350°C and 300°C, respectively. The decrease is due to enhanced scattering associated,

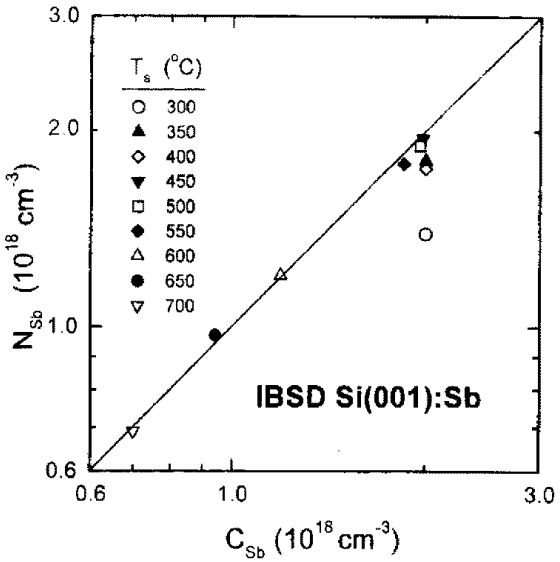

Fig. 2. Sb donor concentrations N_{Sb} determined from Hall measurements vs Sb concentrations C_{Sb} determined from SIMS measurements in homoepitaxial IBSD (Si (001) films grown at T_s=300-700°C.

as noted above, with higher background impurity concentrations at these low T_s and/or residual ion-induced damage not completely annealed out during deposition. These electron transport measurements indicate that essentially all ion-induced damage produced during IBSD is annealed out during deposition even at growth temperatures as low as 400°C consistently with molecular dynamic simulations [19].

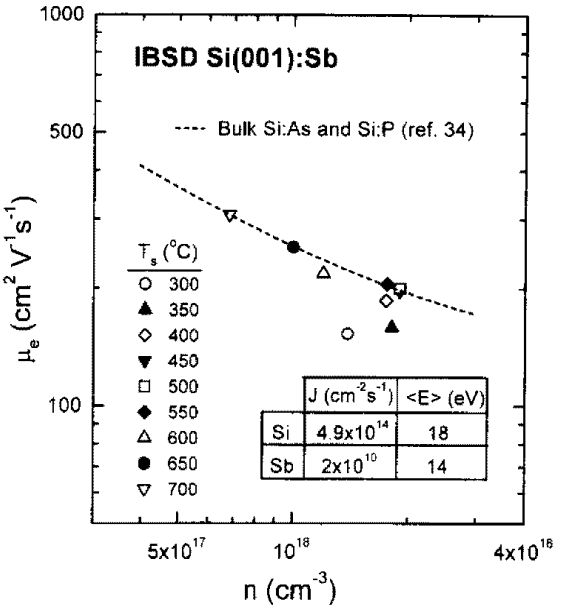

Fig. 3. Room-temperature electron mobilities μ_e vs electron carrier concentrations n in homoepitaxial IBSD Si(001) films grown at T_s=300-700°C. Data from bulk Si (ref. 34) are also shown for comparison.

B. Si(001) layers grown at very low temperatures, T_s=80-300°C

A series of undoped and Sb-doped epitaxial Si (001) layers were also grown at very low temperatures, T_s=80-300°C, with R=0.1 nm-s^{-1} in order to investigate the effects of hyperthermal beams on critical epitaxial thicknesses t_e. Typical high-resolution XTEM micrographs from undoped films showed that the initial layer, epitaxial and defect free in both low-magnification and high-resolution XTEM, is followed by a defective, but still epitaxial, region containing 111 stacking faults [24]. The terminal region is amorphous. Locally, however, the transition from epitaxial to amorphous was always atomically abrupt. The width of the defective epitaxial region, and number density of 111 stacking faults, decreases with decreasing T_s until at $T_s < 150$°C, the faults are not observed.

Fig. 4 shows average total epitaxial thicknesses t_e, obtained from XTEM analyses of undoped and Sb-doped films grown with R=0.1 nm-s^{-1}. Even with slightly higher growth rates, t_e values for undoped Si films grown with $\langle E_{Si} \rangle \simeq 18$ eV are much larger than those of the MBE layers [25] by factors ranging between 5 and 10 over the T_s range investigated.

Low-temperature epitaxy proceeds under conditions where a significant fraction of adatoms condensing on the tops of islands cannot cross step edges to lower terraces before being joined by another adatom and nucleating a new higher-level island. As growth continues and the multilevel islands coalesce, trenches are formed between the islands and become deeper and wider as growth proceeds. Filling of interisland trenches and postponing or avoiding facet formation, is a critical step for ensuring continued epitaxial

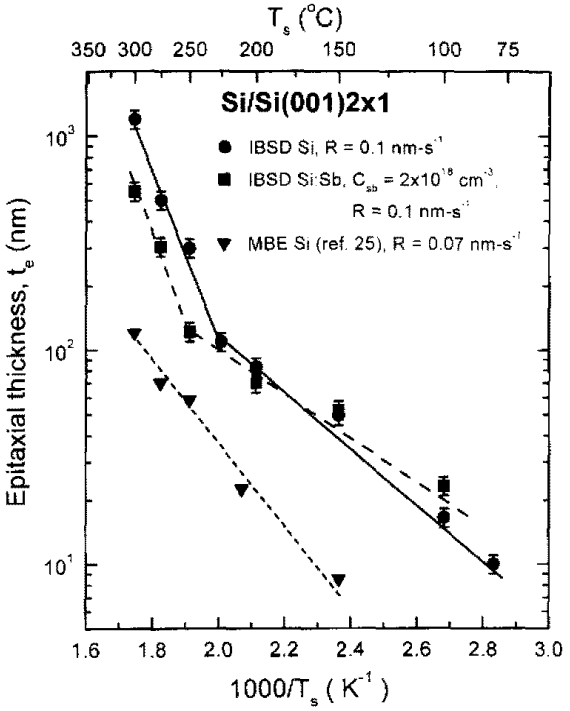

Fig. 4. Epitaxial thicknesses te of undoped and Sb-doped Si(001) films, grown by IBSD using hyperthermal Si and Sb beams as a function of T_s. Film growth rates were R=0.1 nm-s^{-1}. Data from undoped MBE Si(001) films grown at R=0.07 nm-s^{-1} (ref. 25) are also shown for comparison.

growth. We attribute the increase in t_e observed during IBSD primarily to continuous filling of interisland trenches through recoil and forward sputtering processes initiated by the hyperthermal condensing species. This, in turn, minimizes atomic shadowing and inhibits the formation of facetting and nucleation of the amorphous phase. Collisionally-induced enhanced adatom mobilities may also play a role.

Energetic condensing Si atoms collisionally dissociate surface dimers, thus resulting in higher adatom densities on all exposed levels. This effect is not significant at higher growth temperatures as thermal diffusivities overcome the excess supersaturation associated with the concentration of collisionally-formed adatoms. However, at sufficiently low growth temperatures ($\leq$225°C for our growth conditions), this leads, on a given level, to an increased 2D gas supersaturation which in turn results in higher island nucleation rates and, therefore, enhanced interlayer mass transport resulting from increased island-edge crossing probability caused by higher visiting frequencies of adatoms to the island edges of the smaller islands. This, in turn, increases epitaxial thicknesses resulting in the change observed in the slope of the log(t_e) vs 1/T_s curve in Fig. 4.

The $t_e(T_s)$ values were also determined for Sb-doped Si films with $C_{Sb}=2\times10^{18}$ cm^{-3} and the results are presented in Fig. 4. Small Sb fluxes, $J_{Sb}=2\times10^{10}$ cm^{-2}-s^{-1}, corresponding to a steady-state surface coverage of only 4×10^{-5} ML, during low-temperature Si growth decrease epitaxial thicknesses by approximately a factor of two at T_s=250~300°C. This is consistent with the results of AFM images (not shown here) indicating an increased rate of surface roughening.

3.2 Low-temperature epitaxial growth of $Si_{1-x}Ge_x$ alloys

A. Microstructure and crystalline quality of strained alloys

A combination of TEM, XTEM, HR-XRD, and RBS channeling were used to examine the microstructure, crystalline quality, and the degree of relaxation of $Si_{1-x}Ge_x$(001) alloys grown at T_s= 300-550°C with thicknesses t between 30 nm and 0.8 μm.

Plan-view TEM and XTEM images of fully strained $Si_{0.85}Ge_{0.15}$ layers grown even at T_s= 300°C showed no indication of interfacial misfit dislocations. The 110 HR-XTEM images also revealed the films to be highly perfect with no visible extended defects or residual damage. The 111 lattice fringes are continuous across the film/substrate interface with no indication of disorder.

Typical HR-XRD scans from the fully-strained 450-nm-thick epitaxial $Si_{0.85}Ge_{0.15}$ layer grown on Si(001) at T_s=300°C are presented in Figs. 5(a) and 5(b). The full width at half-maximum (FWHM) intensity $\Gamma_{\omega\text{-}2\theta}$ of the 004 alloy peak in the ω–2θ scan in Fig. 5(a) is 32 arc-s which is

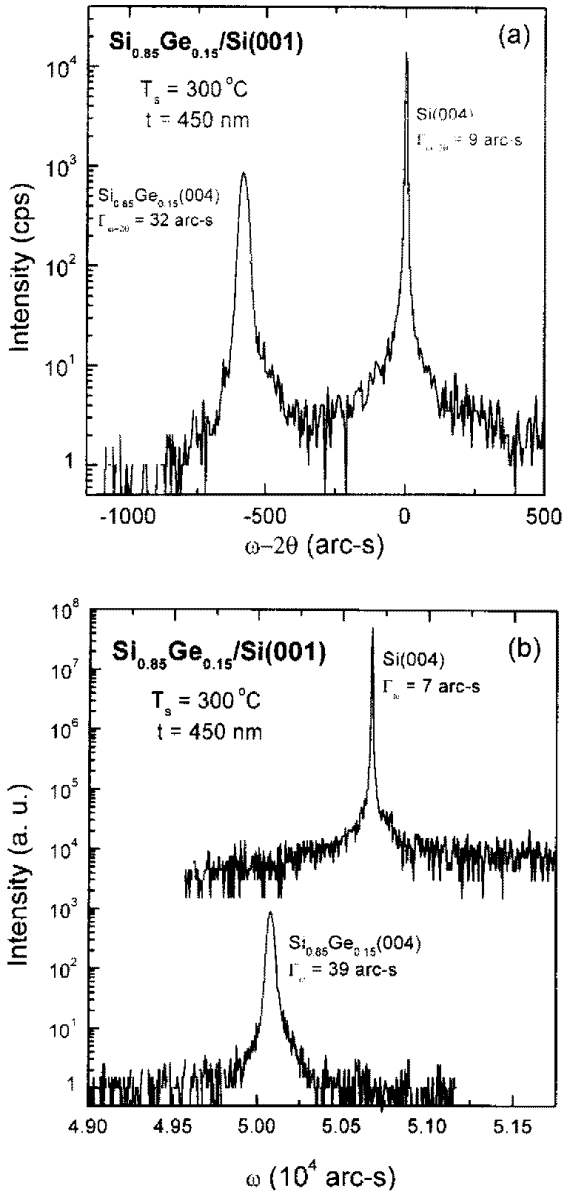

Fig. 5. HR-XRD (a)ω-2θ scan and (b)ω-rocking curve from a fully-strained 450-nm-thick epitaxial $Si_{0.85}Ge_{0.15}$ layer grown on Si(001) at T_s=300°C.

quite close to the minimum theoretical value for this alloy, 23 arc-s, calculated based upon the intrinsic peak width, ≃6 arc-s [26], while accounting for strain broadening due to the lattice-constant mismatch and finite thickness effects [27]. This indicates that the film, even though grown at low temperature, 300°C, is of very high crystalline quality.

An ω rocking curve scan from the same alloy sample, with a FWHM Γ_ω of 39 arc-s, is given in Fig. 5(b). The x-ray in-plane coherence length Δx, a measure of the average mosaic domain size, can be estimated from the experimental Γ_ω value as

$$\Delta x = \frac{2\pi}{|\Delta g_\perp|} \tag{2}$$

where $\Delta g_\perp$ is the width of the diffraction peak defined as

$$|\Delta g_\perp| = \left(\frac{4\pi}{\lambda}\right)\Gamma_\omega \sin\left(\frac{2\theta}{2}\right) \tag{3}$$

in which λ is the x-ray wavelength, $\lambda_{Mo,K}$=0.07107 nm, and 2θ is the 004 Bragg angle, 30.36°. Equations (2) and (3) yield a Δx value of 718 nm for the low-growth-temperature strained $Si_{0.85}Ge_{0.15}$ alloy. This compares very well to the value, Δx=1218 nm, calculated for a film with the minimum theoretical Γ_ω value of 23 arc-s. The substrate, with Γ_ω=7 arc-s, has a Δx value of 3.9 μm.

Fig. 6 is a plot of Γ_ω and Δx values from 450-nm-thick $Si_{0.85}Ge_{0.15}$ alloys as a function of film growth temperature T_s. Γ_ω decreases (and, hence, Δx increases) with increasing T_s to reach a minimum at 450°C for which Γ_ω=26 arc-s (Δx=1167 nm), essentially equal to the minimum theoretical value. At higher growth temperatures, Γ_ω increases slightly due, primarily, to partial strain relaxation.

RBS channeling and rocking curves were also used to access the crystalline quality of strained layers. Typical backscattering spectra obtained along [001] and [011] directions, as well as random dechanneling directions, are shown in Fig. 7 for 450-nm-thick $Si_{0.85}Ge_{0.15}$ layers grown at T_s=300°C. The Ge peaks are abrupt in all spectra and well separated from the Si edges. Moreover, film composition and the degree of ordering are uniform with film depth. Si and Ge minimum [001] yields χ_{min}[001], the ratios of backscattering yields in aligned and random directions obtained from Fig. 7(a), were found to be 4.4 and 4.0% for the 300°C film. Theoretical χ_{min}[001] values

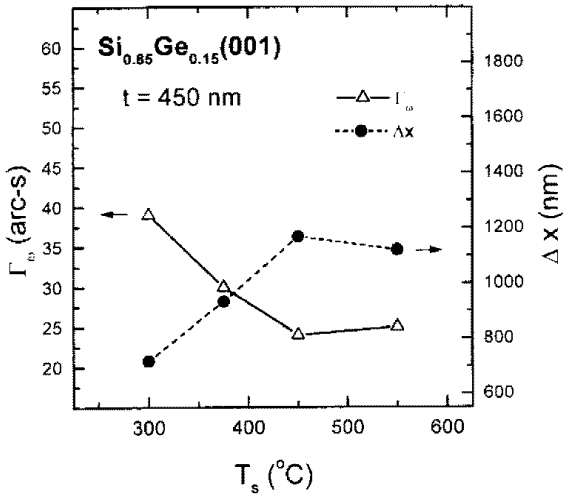

Fig. 6. FWHM ω-rocking curve values Γ_ω and x-ray coherence lengths Δx obtained from 450-nm-thick epitaxial $Si_{0.85}Ge_{0.15}$ alloys grown on Si(001) as a function of deposition temperature T_s.

for bulk single-crystal Si and Ge wafers are 3.1 and 3.6% [28]. For comparison, previously reported Ge χ_{min}[001] values for strained 100-nm-thick MBE $Si_{0.9}Ge_{0.1}$ and $Si_{0.8}Ge_{0.2}$ layers grown at T_s=400°C were 13 and 14%, respectively [14], while a Ge χ_{min}[001] value of 3.2% was reported for 100-nm strained MBE $Si_{0.85}Ge_{0.15}$ grown at T_s= 550°C.

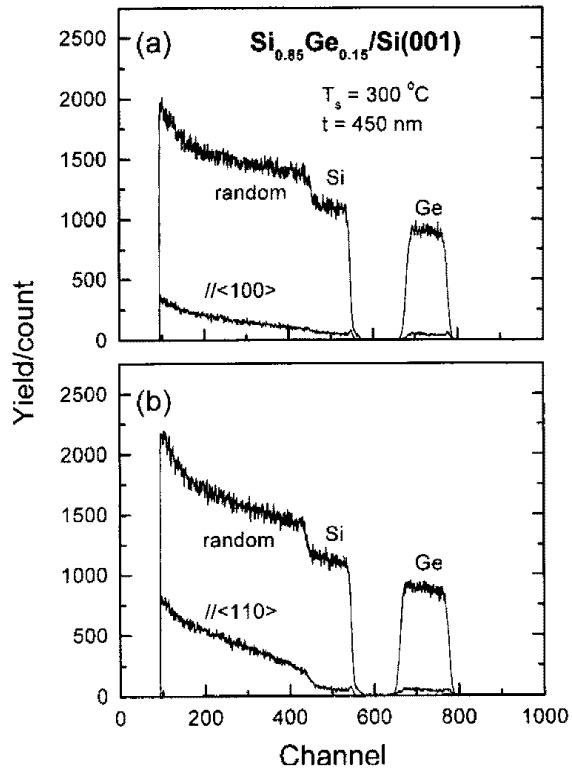

Fig. 7. RBS (a) 001 and (b) 011 channeling spectra from a 450-nm-thick $Si_{0.85}Ge_{0.15}$ layer grown on Si(001) at T_s=300°C. Randomly aligned spectra are also shown for comparison.

Si and Ge χ_{min}[011] values obtained from Fig. 7(b) were found to be 4.0 and 3.6% at T_s=300°C compared to theoretical bulk values of 2.1 and 2.52% [28]. Thus, measured χ_{min} values for both [001] and [011] are indicative of very high quality heteroepitaxial alloy films, even at T_s= 300°C, with Ge substitutionally incorporated at Si lattice sites. Values obtained at the higher growth temperature were even slightly better. The abrupt increase in the Si [011] channeling yields at depths corresponding to the film/substrate interfaces in Figs. 7(b) and the lack of abrupt increases in the [001] aligned spectra (Figs. 7(a)) are due to the tetragonal strain in the films.

RBS axial angular yield profiles, which are more sensitive than channeling spectra to lattice-atom displacements and interstitial defects, were obtained by rocking the samples in random directions about the [001] and [011] axes. Results for the 450-nm-thick T_s=300 and 450°C $Si_{0.85}Ge_{0.15}$ films are shown in Figs. 8(a) and 8(b). Dechanneling effects due to atoms displaced from lattice sites tend to decrease measured channel widths leading to narrower axial yield profiles with smaller intensity differences. The most probable positions for interstitials in Si are open tetrahedral sites. Such defects are shadowed in the [001] and [111] channeling directions, but blocking in the [011] direction. Thus, the presence of interstitials is characterized by "flux peaking," or large increases in backscattering yields above random values, in 110 axial scans [29]. Flux peaking was easily observed, for example, during measurements of Yb-implanted Si wafers [30].

There was no evidence of 110 flux peaking in the present experiments. In fact, the [001] and [011] axial angular yield profiles were quite similar, with no significant narrowing, for both the

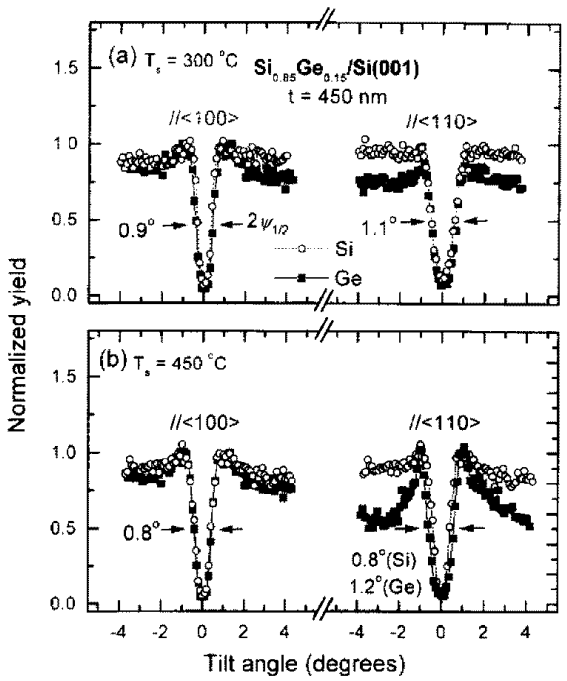

Fig. 8. RBS angular yield profiles about the [001] and [011] directions of 450-nm-thick epitaxial $Si_{0.85}Ge_{0.15}$ films grown on Si(001) at (a) T_s=300°C and (b) T_s=450°C.

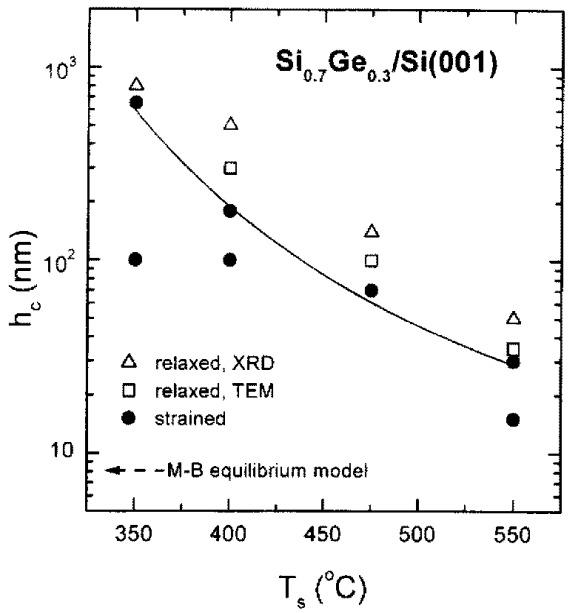

Fig. 9. Critical layer thicknesses hc for epitaxial $Si_{0.70}Ge_{0.30}$ layers grown on Si(001) by UHV IBSD as a function of T_s.

300 and 450°C samples. Si and Ge axial half-angles, $\psi_{1/2}$, defined as the angular half-widths of the profiles at yields halfway between minimum values and the yields for random incidence, were found to be 0.40 and 0.45° for 300°C films compared to theoretical values for pure Si and Ge bulk wafers of 0.57 and 0.73° [28]. Increasing T_s to 450°C had essentially no measurable effect on $\psi_{1/2}$ as shown in Fig. 8.

B. T_s-dependent critical layer thicknesses of $Si_{0.7}Ge_{0.3}$(001)

XRD and Plan-view TEM and XTEM were used to determine critical layer thicknesses h_c of $Si_{0.7}Ge_{0.3}$ alloys as a function of T_s and the measured values are shown in Fig. 9. The resolution for detecting lattice-constant misfit in the present XRD measurements is $\simeq 5\times10^{-4}$ corresponding to a linear dislocation density of 2.5×10^4 cm^{-1} or an average dislocation separation of $\simeq$0.4 μm. Direct observation by TEM is limited to dislocation densities 5×10^3 cm^{-1} or residual in-plane strains $\gtrsim10^{-4}$.

Even at the highest growth temperature used in the present experiments, T_s=550°C, we obtain a critical thickness value of $\simeq$35 nm, a factor of 4 higher than the equilibrium value, $h_{c,eq}$ $\simeq$8 nm, estimated by the Matthews and Blakeslee equilibrium model [11]. This is in good agreement with previous MBE results, using thermal growth beams, in which the films were analyzed by RBS [14]. Obtaining critical thicknesses higher than equilibrium values is generally interpreted as being due to kinetic limitations in dislocation nucleation and propagation. If this is the case, h_c would be expected to increase still further at lower growth temperatures. The data in Fig. 9 show that h_c indeed increases rapidly with decreasing T_s. In fact, at T_s=350°C we obtain h_c = 650 nm, an increase by more than an order of magnitude over h_c(550°C). This is, by far, the highest h_c value yet reported for $Si_{0.70}Ge_{0.30}$ layers.

Differences between experimental and theoretical h_c values are partially due to limited experimental resolution for detecting the initiation of interfacial relaxation [10]. However, the present results show that the ratio $h_c/h_{c,eq}$ increases

rapidly as T_s is decreased below 550°C until at T_s =350°C, we obtain $h_c/h_{c,eq}$=85. This very large increase is primarily due to the kinetic suppression of thermally-activated dislocation nucleation and, to a lesser extent, propagation [12]. LeGoues *et al.* [31] obtained a dislocation nucleation activation barrier of 5 eV in $Si_{1-x}Ge_x(001)$ (x= 0.15~0.45) grown by UHV-CVD. Reported activation barriers for dislocation glide in $Si_{1-x}Ge_x$ alloys with x=0.15-0.30 as used in the present experiments range from 1.6 to 2.25 eV [32, 33].

4. CONCLUSIONS

TEM, SIMS, and T-dependent Hall measurements Sb-doped Si(001) films at T_s as low as 400°C showed that dopant species are incorporated with complete electrical activity and carrier mobilities are equal to the best values reported for bulk Si. Sb incorporation probabilities are one to three orders of magnitude higher than in MBE Si films. At very low growth temperatures, T_s=80-300°C, the use of energetic, rather than thermal, Si beams during deposition was found to dramatically increase Si(001) epitaxial thicknesses t_e by up to an order of magnitude. The presence of even small coverages of Sb at T_s=250-300°C decreases t_e.

A combination of plan-view and XTEM, HR-XRD, RBS channeling, and axial angular-yield profiles demonstrated that the $Si_{1-x}Ge_x(001)$ alloy films, with $0.15 \leq x \leq 0.30$, are of extremely high crystalline quality. Critical layer thicknesses h_c for strain relaxation in these alloys were found to increase rapidly with decreasing growth temperature. For $Si_{0.70}Ge_{0.30}$, h_c ranged from 35 nm at $T_s = 550$°C to 650 nm at 350°C compared to an equilibrium value of $\simeq 8$ nm.

Acknowledgements

The authors gratefully acknowledge the partial financial support of the Joint Services Electronics Program, the Semiconductor Research Corporation, and the Materials Science Division of the Department of Energy, USA, during the course of this research. We also would like to thank Dr. M. Sardela Jr. and M. Matsuoka for their help in x-ray diffraction and RBS measurements, respectively.

References

1. M. A. Hasan, J. Knall, S. A. Barnett, A. Rockett, J.-E. Sundgren, and J. E. Greene, J. Vac. Sci. Technol. A **5**, 1883 (1987).
2. C. H. Choi, L. Hultman, and S. A. Barnett, J. Vac. Sci. Technol. A **8**, 1587 (1990).
3. W.-X. Ni, J. Knall, M. A. Hasan, J.-E. Sundgren, L. C. Markert, and J. E. Greene, Phys. Rev. B **40**, 10449 (1989).
4. L. C. Markert, J. E. Greene, W.-X. Ni, G. V. Hansson, and J.-E. Sundgren, Thin Solid Films **59**, 206 (1991).
5. J.-E. Sundgren, J. Knall, W.-X. Ni, M.-A. Hasan, L. Markert, and J. E. Greene, Thin Solid Films **183**, 281 (1989).
6. J. C. Bean, Proc. IEEE **80**, 571 (1992).
7. K. Sakamoto, T. Sakamoto, S. Nagao, G. Hashiguchi, K. Kuniyoshi, and Y. Bando, Jap. J. Appl. Phys. **26**, 666 (1987).
8. X. Wei, G. L. Zhou, C. Sheng, M. R. Yu, and X. Wang, Vacuum **43**, 1035 (1992).
9. D. J. Godbey, J. V. Lill, J. Deppe, and K. D. Hobart, Appl. Phys. Lett. **65**, 711 (1994).
10. S. C. Jain, J. R. Willis, and R. Bullough, Adv. Phys. **39**, 127 (1990).
11. J. W. Matthews andA. E. Blakeslee, J. Cryst. Growth **27**, 118 (1974), **32**, 265 (1976).
12. B. W. Dodson, Appl. Phys. Lett. **53**, 37 (1988).
13. R. Hull and J. C. Bean, CRC Critical Rev. Solid State Mater. Sci. **17**, 507 (1992).
14. J. C. Bean, L. C. Feldman, A. T. Fiory, S. Nakahara, and I. K. Robinson, J. Vac. Sci. Technol. A **2**, 436 (1984).
15. E. Kasper, H.-J. Herzog, and H. Kibbel, Appl. Phys. **8**, 199 (1975).
16. J. Tersoff and F. K. LeGoues, Phys. Rev. Lett. **72**, 3570 (1994).

17. D. J. Eaglesham, H.-J. Gossmann, and M. Cerullo, Phys. Rev. Lett. **65**, 1227 (1990).
18. N.-E. Lee, David G. Cahill and J. E. Greene, J. Appl. Phys. **80**, 2199 (1996).
19. M. Kitabatake and J. E. Greene, J. Appl. Phys. **73**, 3183 (1993).
20. C. Weissmantel, G. Hecht, and H. J. Hinneberg, J. Vac. Sci. Technol. **17**, 812 (1980).
21. W. M. Lau, I. Bello, L. J. Huang, X. Feng, M. Vos, and I. V. Mitchell, J. Appl. Phys. **74**, 7101 (1993).
22. L. C. Markert, Ph.D. Thesis, University of Illinois at Urbana-Champaign, 1991.
23. C. M. Wolfe, N. Holonyak, Jr., and G. E. Stillman, *Physical Properties of Semiconductors* (Prentice-Hall, Englewood Cliffs, NJ, 1989), p. 343.
24. N.-E. Lee, G. Xue, and J. E. Greene, J. Appl. Phys. **80**, 769 (1996).
25. D. J. Eaglesham, H.-J. Gossmann, and M. Cerullo, Phys. Rev. Lett. **65**, 1227 (1990).
26. P. Fewster, J. Appl. Cryst. **22**, 64 (1989).
27. J. Lee, W. E. Mayo, and T. Tsakalakos, J. Electr. Materials **21**, 867 (1991).
28. W.-K. Chu, J. W. Mayer, and M.-A. Nocolet, *Backscattering Spectroscopy* (Academic Press, New York, 1978) p. 232.
29. The detection limit of this technique is $\sim 10^{-3} Z_h^2/Z_i^2$ (ref. 28) where Z_h and Z_i are the atomic numbers of the host and interstitial species, respectively. For Ge in Si, this corresponds to $\simeq 9\times 10^{18}$ cm^{-3}.
30. J. U. Anderson, O. Anderson, J. A. Davis, and E. Uggeroj, Rad. Effect **7**, 25 (1971).
31. F. K. LeGoues, P. M. Mooney, and J. Tersoff, Phys. Rev. Lett. **71**, 396 (1993).
32. C. G. Tuppen and C. J. Gibbings, J. Appl. Phys. **68**, 1526 (1990).
33. D. C. Houghton, J. Appl. Phys. **70**, 2136 (1991).
34. G. Masetti, M. Severi, and S. Silmi, IEEE Trans. Elec. Dev. **ED-30**, 764 (1983).